Title

Survival and Functionality of hESC-Derived Retinal Pigment Epithelium Cells Cultured as a Monolayer on Polymer Substrates Transplanted in RCS RatsRetinal Pigment Epithelium Transplantation

Journal

Investigative Ophthalmology & Visual Science, 57(6)

ISSN

0146-0404

Authors

Thomas, Biju B

Zhu, Danhong

Zhang, Li

et al.

Publication Date

2016-05-27

DOI

10.1167/iovs.16-19238

Peer reviewed

Survival and Functionality of hESC-Derived Retinal Pigment Epithelium Cells Cultured as a Monolayer on Polymer Substrates Transplanted in RCS Rats

Biju B. Thomas,[1,2] Danhong Zhu,[1,3] Li Zhang,[4] Padmaja B. Thomas,[5] Yuntao Hu,[6] Hossein Nazari,[1] Francisco Stefanini,[1] Paulo Falabella,[1] Dennis O. Clegg,[7] David R. Hinton,[1,3] and Mark S. Humayun[1,2]

[1]Department of Ophthalmology, USC Roski Eye Institute, University of Southern California, Los Angeles, California, United States
[2]USC Institute for Biomedical Therapeutics, University of Southern California, Los Angeles, California, United States
[3]Department of Pathology, Keck School of Medicine, University of Southern California, Los Angeles, California, United States
[4]Eye Center, Second Affiliated Hospital, Medical School of Zhejiang University, Hangzhou, China
[5]Cellular Therapies Production Center, City of Hope, Duarte, California, United States
[6]Department of Ophthalmology, Beijing Tsinghua Changgung Hospital, Tsinghua University Medical Center, Beijing, China
[7]Center for Stem Cell Biology and Engineering, University of California, Santa Barbara, California, United States

Correspondence: Biju B. Thomas, Department of Ophthalmology, University of Southern California, Los Angeles, CA 90033, USA; biju.thomas@med.usc.edu.

Submitted: January 28, 2016
Accepted: April 13, 2016

Citation: Thomas BB, Zhu D, Zhang L, et al. Survival and functionality of hESC-derived retinal pigment epithelium cells cultured as a monolayer on polymer substrates transplanted in RCS rats. *Invest Ophthalmol Vis Sci*. 2016;57:2877–2887. DOI:10.1167/iovs.16-19238

Purpose. To determine the safety, survival, and functionality of human embryonic stem cell–derived RPE (hESC-RPE) cells seeded on a polymeric substrate (rCPCB-RPE1 implant) and implanted into the subretinal (SR) space of Royal College of Surgeons (RCS) rats.

Methods. Monolayers of hESC-RPE cells cultured on parylene membrane were transplanted into the SR space of 4-week-old RCS rats. Group 1 (n = 46) received vitronectin-coated parylene membrane without cells (rMSPM+VN), group 2 (n = 59) received rCPCB-RPE1 implants, and group 3 (n = 13) served as the control group. Animals that are selected based on optical coherence tomography screening were subjected to visual function assays using optokinetic (OKN) testing and superior colliculus (SC) electrophysiology. At approximately 25 weeks of age (21 weeks after surgery), the eyes were examined histologically for cell survival, phagocytosis, and local toxicity.

Results. Eighty-seven percent of the rCPCB-RPE1–implanted animals showed hESC-RPE survivability. Significant numbers of outer nuclear layer cells were rescued in both group 1 (rMSPM+VN) and group 2 (rCPCB-RPE1) animals. A significantly higher ratio of rod photoreceptor cells to cone photoreceptor cells was found in the rCPCB-RPE1–implanted group. Animals with rCPCB-RPE1 implant showed hESC-RPE cells containing rhodopsin-positive particles in immunohistochemistry, suggesting phagocytic function. Superior colliculus mapping data demonstrated that a significantly higher number of SC sites responded to light stimulus at a lower luminance threshold level in the rCPCB-RPE1–implanted group. Optokinetic data suggested both implantation groups showed improved visual acuity.

Conclusions. These results demonstrate the safety, survival, and functionality of the hESC-RPE monolayer transplantation in an RPE dysfunction rat model.

Keywords: transplantation, stem cells, parylene, retinal pigment epithelium, optokinetic testing, superior colliculus

Dysfunction and death of RPE cells have been observed in human degenerative diseases leading to blindness, such as AMD. Age-related macular degeneration is one of the leading causes of blindness in the Western world.[1–3] Although antiangiogenic therapies were developed to treat exudative AMD,[4] there is no effective method for the treatment of dry AMD, particularly its end-stage, geographic atrophy.[5,6] A number of research groups are in pursuit of strategies to replace degenerated RPE cells with healthy RPE cells in the submacular space.[7–16]

Various cell types have been examined for RPE cell replacement. These cells include immortalized cell lines, such as the human RPE cell line ARPE19,[17] sheets of adult RPE,[18] fetal RPE,[19] RPE derived from human embryonic stem cells (hESC-RPE),[20–24] human induced pluripotent stem cell–derived RPE,[9,25,26] and many non-RPE cell lines.[27–37]

Stem cells, with their capacity to differentiate and replace diseased cells, can be an excellent source for RPE transplantation.[10,11,16,28,29,38] Almost all previous studies used the method of cell suspension injection to evaluate the feasibility of stem cell–based RPE replacement therapies. This strategy is dependent on the integration of injected cells into the host RPE monolayer, which has been shown to occur in some studies[39] but not in others.[20] However, when injected as a cell suspension, most cells fail to form a polarized monolayer and survival rates are poor.[40,41] Furthermore, Bruch's membrane,

Investigative Ophthalmology & Visual Science

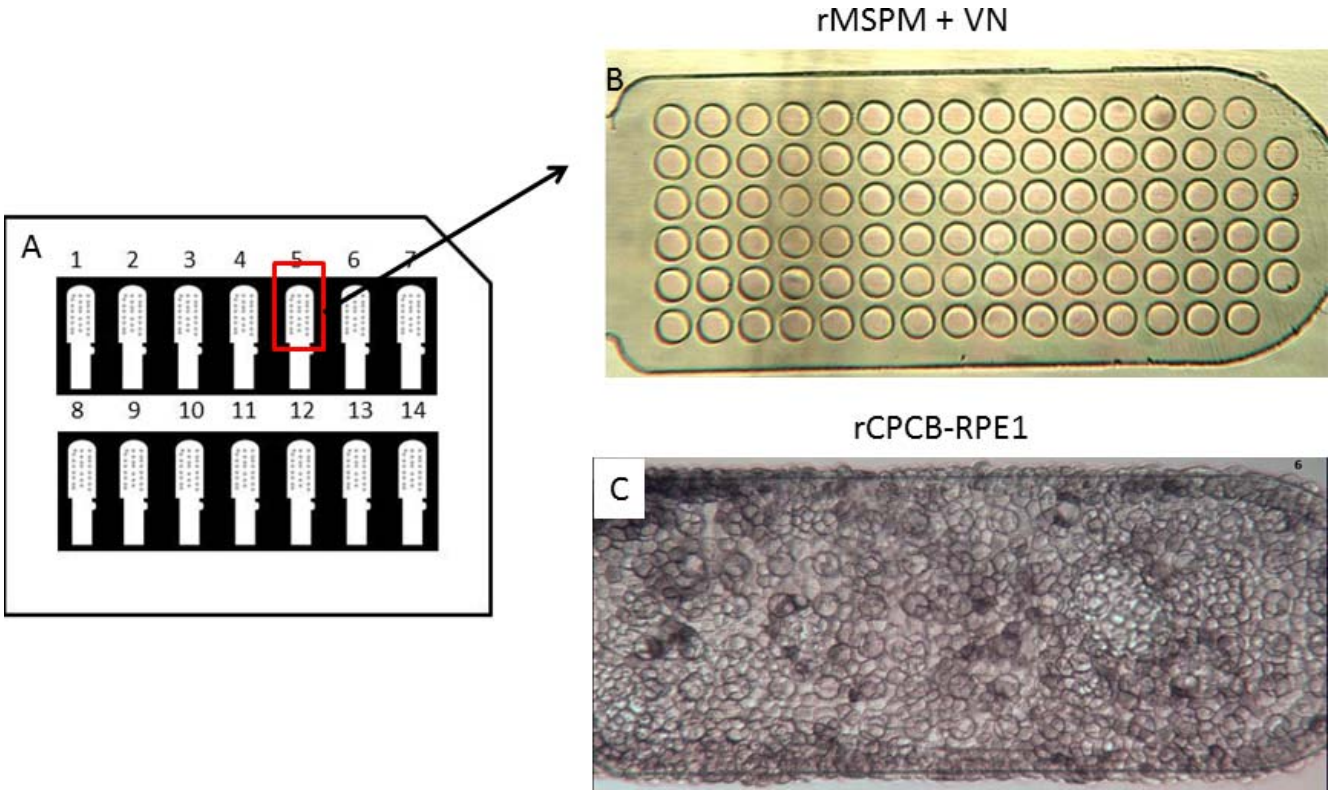

FIGURE 1. Images of rMSPM+VN and rCPCB-RPE1 implants that were used for rat transplantation experiments. (**A**) Diagrammatic representation of a rat parylene frame before cell culture (each frame contains 14 individual parylene implants). (**B**) Image of an individual rat parylene membrane coated with VN (rMSPM+VN). The *circles* are the ultrathin areas of the parylene implant. (**C**) Image of an individual rat-sized CPCB-RPE1 implant 30 days after seeding with hESC-RPE cells (rCPCB-RPE1). Retinal pigment epithelium cells were found to cover the entire surface of the CPCB-RPE1 implant.

the normal substrate for RPE attachment in vivo, has been shown not to support RPE attachment when isolated from AMD-afflicted donor eyes.[42] Hence, RPE cells cultured as a monolayer on a basal substrate might be a better transplantation candidate for repairing damaged RPE.

Both biodegradable and biostable substrates are being studied for RPE cell culture and transplantation.[43–47] We have developed a biostable scaffold composed of the biocompatible xylene-based polymer parylene, which supports RPE monolayer formation and has permeable properties similar to Bruch's membrane.[48] Our previous study demonstrated the safety and long-term survival of polarized monolayer of hESC-RPE cells cultured on ultrathin parylene substrates (rCPCB-RPE1 implant) and transplanted in athymic nude rats.[49] Here, we report on findings of implantation of rCPCB-RPE1 into the subretinal (SR) space of Royal College of Surgeons (RCS) rats, a model of retinal dystrophy. Royal College of Surgeons rats have a mutation in the merTK gene and lack the ability to phagocytose photoreceptor outer segments, resulting in photoreceptor death and loss of vision. It has served as a suitable model for evaluation of the safety and efficacy of the hESC-RPE transplantation.[50] The current investigation demonstrates that monolayers of hESC-RPE implanted in dystrophic RCS rats survive, carry out phagocytosis, rescue photoreceptors, and provide functional visual benefits.

METHODS

Animals

Royal College of Surgeons rat pups (27–29 days old) were divided into an rMSPM+VN (parylene substrate coated with vitronectin)–implanted group (group 1, $n = 46$), an rCPCB-RPE1–implanted group (group 2, $n = 59$), and a nonimplanted control group (group 3, $n = 13$). Immunosuppression procedures consisted of initial dexamethasone injection and oral cyclosporine administration and were performed as per the protocol described by Lu et al.[51] This study was carried out in strict accordance with the ARVO Statement for the Use of Animals in Ophthalmic and Vision Research.

Cell Culture and Preparation of Implants for Transplantation

Human embryonic stem (ES) cells (National Institutes of Health–registered H9 cell line, WiCell Research Institute, Inc., Madison, WI, USA) were cultured in mTeSR1 medium (Stemcell Technologies, Vancouver, BC, Canada). The ES cells were allowed to spontaneously differentiate into RPE cells in serum-free and xeno-free XVIVO 10 medium (Lonza, Walkersville, MD, USA) for 12 weeks.[22,52] The pigmented RPE-like cells were enriched by enzymatic treatment that selectively harvests pigmented cells. The isolated RPE-like cells were dissociated by trypLE (Life Technologies, Grand Island, NY, USA) and cultured in human VN (BD Biosciences, Franklin Lakes, NJ, USA)-coated plates with XVIVO 10 medium. Passage 3 hESC-RPE cells were used to seed on the parylene membranes (rMSPMs; Figs. 1A–C). The parylene substrates used for both rMSPM+VN and rCPCB-RPE1 implants consisted of an ultrathin membrane of parylene (0.30-μm thick) with a 6-μm-thick supporting mesh. Previous in vitro studies suggested that nutrients and macromolecules can diffuse across 0.30-μm parylene-C to nourish the cells.[51] For group 1 studies, rMSPMs were coated with 10 μg/mL VN for 2 hours at room

Table 1. List of Antibodies Used for Immunostaining

Antibodies	Purpose	Manufacturer	Catalog No.	Lot No.	Dilution
TRA-1-85	Human marker	R&D Systems, Minneapolis, MN, USA	MAB3195	WJCO112081	1:100
RPE65	RPE marker	Abcam, Cambridge, MA, USA	Ab105366	GR37628-8	1:500
Rhodopsin	Photoreceptor phagocytosis Identity of rod photoreceptor	Abcam	Ab3267	GR43050-1	1:400
Cone arrestin	Identity of cone photoreceptor	EMD/Millipore, Temecula, CA, USA	AB15282	2392304	1:2000
Ki67	Cell proliferation	Abcam	AB16667	GR59808-2	1:500
Goat anti-mouse IgG conjugated with Rhodamine	Secondary antibody	Jackson ImmunoResearch, West Grove, PA, USA	115-025-146	117098	1:100
Goat anti-rabbit IgG conjugated with FITC	Secondary antibody	Jackson ImmunoResearch	11-095-144	113127	1:100

temperature under sterile conditions. After the VN coating, the membranes were placed in XVIVO 10 for a period 28 to 35 days, a period during which the media was changed twice a week before the implantation procedure. For group 2 studies, rMSPMs were coated with 10 μg/mL VN and then seeded with passage 3 hESC-RPE cells. The cells on the rMSPMs were cultured in XVIVO for 28 to 35 days with medium changes twice a week.

Transplantation Surgery

For the implantation surgeries, the rats were anesthetized and the pupil was dilated with 1% tropicamide (1 drop). After the

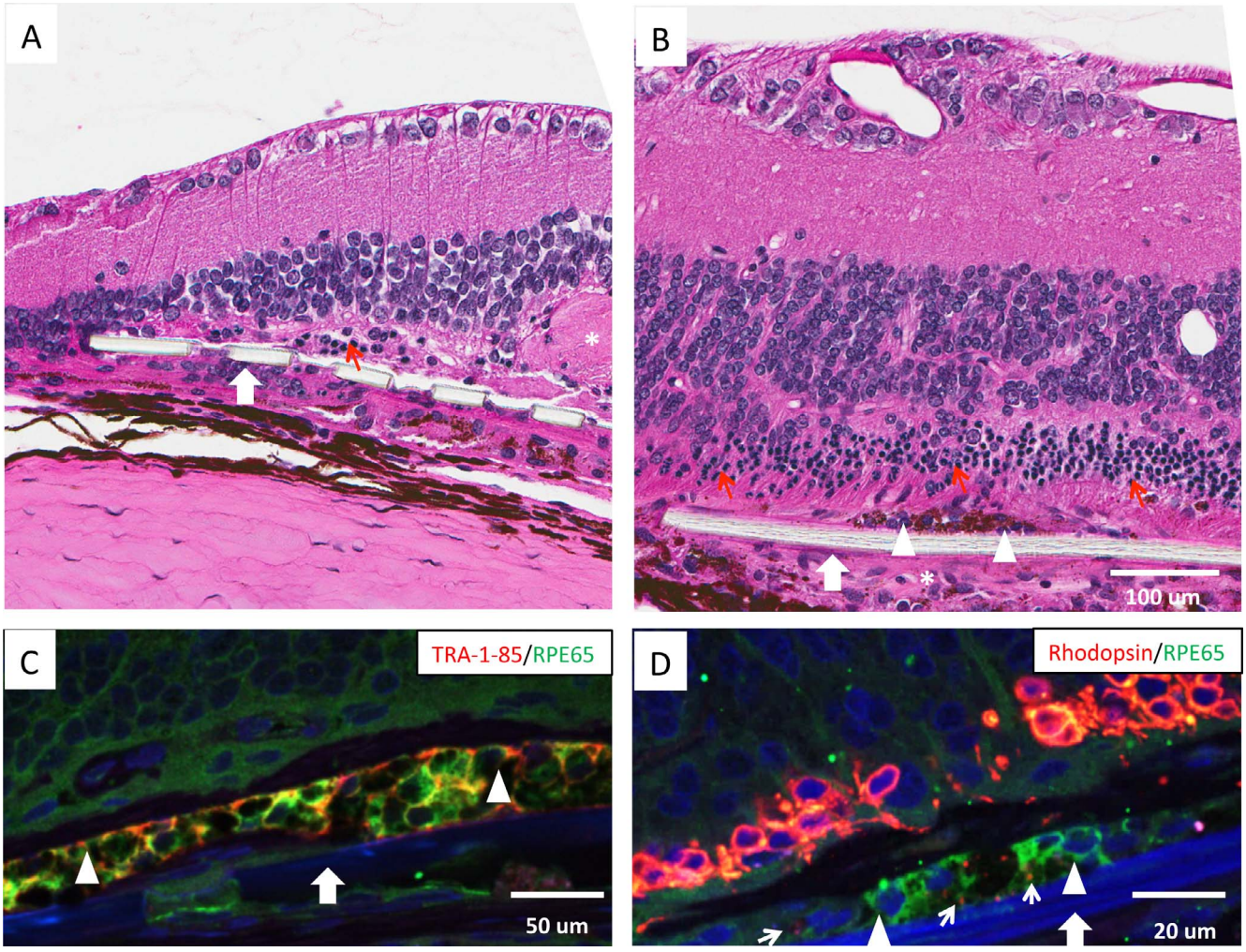

Figure 2. Histologic assessment of rMSPM+VN and rCPCB-RPE1 implants in RCS rats. Representative HE and immunostaining images of rat retina after implantation. Implanted (**A**) parylene membrane (rMSPM+VN) and (**B**) rCPCB-RPE1 in the subretinal space (*large white arrow*), surviving ONL (*red arrows*), and area showing some cellular reaction (*white stars*). Relatively intact host retina, elevated and wavy INL, and focal loss of INL cells can be observed in both (**A**) and (**B**). The choroidal layer that appears to be separated from the remaining retina is considered as a histologic artifact. (**C**) Immunostaining of TRA-1-85/RPE65 shows implanted hESC-RPE cells (*white arrowhead*). (**D**) Rhodopsin immunostaining showing rhodopsin-positive phagosomes inside the implanted RPE65-positive hESC-RPE cells (*small white arrow* pointing to phagosomes).

Table 2. Human ES Cell–Derived RPE Survival in rCPCB-RPE1–Implanted Rats

hESC-RPE Coverage on rCPCB-RPE1 Implants			TRA-1-85 Expression Level				RPE65 Expression Level			
>85%	51%–85%	<50%	+++	++	+	−	+++	++	+	−
$n = 12$	$n = 3$	$n = 8$	$n = 5$	$n = 11$	$n = 4$	$n = 3$	$n = 4$	$n = 10$	$n = 6$	$n = 3$
52.2%	13.0%	34.8%	21.7%	47.8%	17.4%	13%	17.4%	43.5%	26.1%	13%

The degree of hESC-RPE survival in rCPCB-RPE1–implanted rat eyes was examined at 21 weeks postimplantation using HE-stained images and based on TRA-1-85/RPE65 expression. The TRA-1-85/RPE65 expression was graded as negative (–), weak positive (+), moderate positive (++), and strong positive (+++).

conjunctiva was opened, a small incision (approximately 0.8–1.0 mm) was cut transsclerally at the temporal equator of the eye until the choroid was exposed. The anterior chamber was punctured to release some of the aqueous humor to reduce IOP. Approximately 5 μL balanced salt solution was injected into the SR space through a 33-gauge steel needle to create a bleb. The implant was introduced through the subscleral space to reach the area of the SR bleb. Optical coherence tomography (OCT) was performed to confirm placement of the implant. The success of implant placement of group 1 and group 2 was based on a grading system with a scale of 1 to 5, with 5 being the most optimal placement.

Optokinetic Testing and Superior Colliculus (SC) Electrophysiology

Optokinetic (OKN) testing was performed at four different time points after surgery in accordance with previous publication.[53] An EthoVision XT, Noldus Information Technology (Wageningen, The Netherlands) computer program was used to generate alternate black and white stripes. The head-tracking responses during clockwise (1 minute) and anticlockwise (1 minute) stripe rotations were recorded using a digital camcorder. Visual acuity was tested by the decrease of stripe width at 0.5 decrements. Video recordings were evaluated to compute the head-tracking scores by two separate investigators who were both blind to the experimental condition. Electrophysiological mapping of the SC was performed at approximately 21 weeks postsurgery.

During SC mapping, the responses were recorded from approximately 30 different SC locations. At each location, the recordings were made at varying light intensity (~0.25 steps) to obtain a luminance threshold map of the SC as described previously.[54–56]

Histologic Assessments

Eyes from approximately half of the rCPCB-RPE1 animals were collected within 2 hours after light onset and stained with antibodies to rhodopsin to identify phagocytosed rod photoreceptor segments. The remaining animals from the rCPCB-RPE1 group underwent SC electrophysiology and were not considered for phagocytosis studies. All eyes were fixed in 10% buffered formalin, embedded in paraffin and cut 5 μm in thickness in a microtome. Hematoxylin-eosin (HE) staining was performed on the slides of every eye. The HE-stained slides were scanned and photographed using an AperioScanscope CS (Aperio Technologies, INL., Vista, CA, USA) microscope. The percentage of cell coverage area was calculated based on the total length of the implant and the length of the implant area covered by RPE cells.

For immunostaining, all slides were deparaffinized, rehydrated, and antigen retrieved (sodium citrate, pH 6.0). After staining, the slides were mounted with fluorescent-enhanced mounting medium with 4′,6-diamidino-2-phenylindole (DAPI) (Vector Laboratory, Burlingame, CA, USA). Details of the antibodies used are included in Table 1. All images were taken using the Ultraviewer ERS dual-spinning disk confocal microscope (PerkinElmer, Waltham MA, USA) equipped with a C-Apochromat (Carl Zeiss, Thornwood, NY, USA) ×10 high dry lens, a C-Apochromat ×40 water immersion lens NA 1.2, and an electron multiplier charge-coupled device cooled digital camera (Hamamatsu Orce_ERCC [12 bit camera]; PerkinElmer, Waltham, MA, USA). Images were captured and processed using PerkinElmer Velocity imaging software.

Outer Nuclear Layer (ONL) Cell Count

Hematoxylin-eosin–stained images were used to count the ONL cells. The rescued ONL cell count was performed in three areas of each section (i.e., the entire apical side of the implant and 100-μm area from adjacent sides of the implant). All counts were normalized to a standard implant length. For each eye, the final ONL cell count (for each of the above three areas) represented the average of the values from a minimum of three different levels of the implanted eye. The "Nuclear V.09" algorithm (Aperio microscope software) was used in the cell count. Three sections from comparable levels were evaluated in control animals.

Assessment of Rod/Cone Ratio

Cells were stained for rhodopsin or cone arrestin. Immunopositive rhodopsin or cone arrestin cells located between the inner nuclear layer (INL) and the implant were manually counted and the data were normalized for each sample. Rod/cone cell counts were determined using the rhodopsin and cone arrestin double-stained images. The ratio was determined by determining number of rods/number of cones.

Statistics

Statistical comparisons were made with Student's *t*-test or ANOVA followed by appropriate post hoc test using Graphpad Prism software (Graphpad Software, Inc., La Jolla, CA, USA).

Table 3. Rod/Cone Ratio in rCPCB-RPE1–Implanted Rats and rMSPM+VN–Implanted Rats

Groups	Rod/Cone Ratio >3	Rod/Cone Ratio 1.5–2.9	Rod/Cone Ratio 1.0–1.5	Rod/Cone Ratio <1
rCPCB-RPE1 animals, *n*	4	8	5	6
rMSPM+VN animals, *n*	0	1	9	5

The rod/cone ratio was considerably higher in the rCPCB-RPE1–implanted rats compared with the rMSPM+VN–implanted group. In most of the rCPCB-RPE1–implanted rats (12/21), a rod/cone ratio higher than 1.5 was observed.

Investigative Ophthalmology & Visual Science

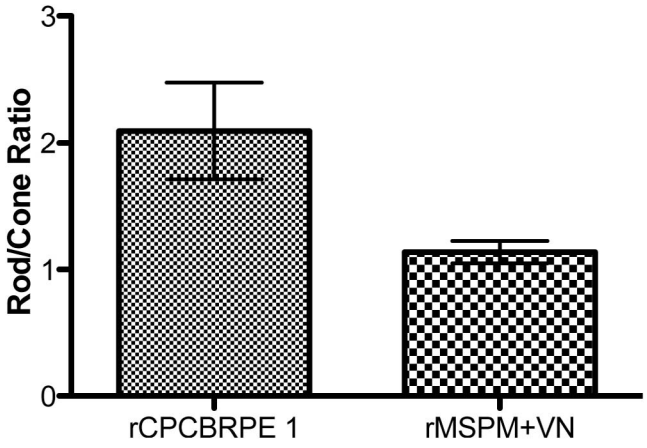

FIGURE 3. Rod/cone ratio in rMSPM+VN– and rCPCB-RPE1–implanted RCS rats (mean ± SE). Statistical comparison performed using Student's *t*-test showing significantly higher rod/cone ratio in rCPCB-RPE1–implanted RCS rats ($P < 0.05$).

For all comparisons, the significance level was determined at $P < 0.05$.

RESULTS

Using the OCT to screen for proper implant placement, animals with the substrate placed as a flat sheet adjacent to the Bruch's membrane was selected for further analysis. Based on OCT images, 17 animals (17/46) were selected from group 1 (rMSPM+VN) and 23 animals (23/59) were selected from group 2 (rCPCB-RPE1). All of the group 2 animals (rCPCB-RPE1) had a well-pigmented, intact hESC-RPE cell monolayer attached to the parylene substrate.

No major chronic inflammation was observed in any of the implanted animals. When rMSPM+VN (representative image: Fig. 2A) or rCPCB-RPE1 (representative image: Fig. 2B) implants were placed entirely in the SR space, most of the retinas (95.0%) maintained basic structure without major structural damage. Both groups showed an elevated and wavy INL and focal loss of INL cells (Figs. 2A, 2B). All eyes in group 1 and group 2 showed preservation of the ONL. No such ONL preservation was apparent in the control RCS rats.

The percentage of parylene still covered by hESC-RPE at 21 weeks postimplantation was assessed based on histologic images from serial sections. In most of the implanted eyes (12/23), more than 85% of the parylene showed hESC-RPE cell coverage (Table 2). Cells positive for TRA-1-85 and RPE65 were found in 87% of samples. This further demonstrated that the implanted RPE cells survived for up to 21 weeks post-implantation (Table 2; Figs. 2C, 2D). Phagocytosis study results revealed that six of the seven samples showed implanted RPE cells containing rhodopsin-positive particles (Fig. 2D).

Although no ONL cells were found in the age-matched RCS rat control group (without surgery), significant numbers of ONL cells were rescued in both rCPCB-RPE1– and rMSPM+VN–implanted groups. No significant differences were found in the number of rescued ONL cells between the rCPCB-RPE1– and rMSPM+VN–implanted groups (146 ± 69 vs. 170 ± 88, $P > 0.05$).

The rescue of rods and cones was found both in rCPCB-RPE1–implanted rats and rMSPM+VN–implanted rats with a more robust rod recuse observed in the rCPCB-RPE1–implanted group as evidenced by immunohistochemistry. Not only more rod survival (compared with cones) was observed in the rCPCB-RPE1–implanted rats (74% of the rCPCB-RPE1 rats versus 67% of the rMSPM+VN–implanted rats), but also the degree of rod preservation was higher in the rCPCB-RPE1 group (Table 3). Although most of the rCPCB-RPE1–implanted rats (12/21) showed rod/cone ratio greater than 1.5, only one rat in the rMSPM+VN–implanted group (1/15) showed rod/cone ratio greater than 1.5. The higher rod/cone ratio observed in the rCPCB-RPE1 group was statistically significant ($P < 0.05$, Student's *t*-test, Fig. 3). As shown in Figures 4A and 4B, better differentiation and alignment of photoreceptors as well as their inner segments (IS) and outer segments (OS) are observed in the rCPCB-RPE1–implanted animals. Cell proliferation has not occurred in the implanted cells, as evidenced by the absence of staining for Ki67, a marker of proliferation (Fig. 5).

The SC mapping data suggested that visual activity was almost absent in the control (nonimplanted) animals (Fig. 6C), whereas some weak residual visual activity was observed in the SC of rMSPM+VN RCS rats (Fig. 6A). Strong visual activity (responses recorded during low-light level stimulation) was observed in the SC of rCPCB-RPE1–implanted animals (Fig. 6B). Interestingly, in these animals, the responses were recorded from an area corresponding to the quadrant of the eye in which implants were placed. Among the number of SC locations responding at various levels of light stimulation, a significantly higher number of SC sites in the rCPCB-RPE1–implanted animals showed visual responses (Fig. 7). The luminance threshold level was considerably lower ($P < 0.05$) in the rCPCB-RPE1–implanted rats when compared with rMSPM+VN–implanted animals.

Optokinetic testing revealed significantly higher visual acuity in the implanted eyes ($P < 0.05$, paired *t*-test) from both rMSPM+VN– and rCPCB-RPE1–implanted groups during the assessment performed at 13 weeks and 21 weeks postimplantation (Fig. 8).

DISCUSSION

The results from our study support the safety and potential bioactivity of the rCPCB-RPE1 implant. Based on histologic assessments and immunostaining data (Table 2; Figs. 2C, 2D), good coverage of the implanted hESC-RPE cells on the parylene membrane and its survival in the rat subretinal space up to 21 weeks postimplantation is clearly demonstrated in this study. The implanted hESC-RPE cells remained as a monolayer on the surface of the parylene substrate and there was no evidence of cell migration or proliferation after implantation. A human specific marker (TR-1-85) confirmed that the implanted hESC-RPE cells are present only at the location of the implant. Cell proliferation has not occurred in the implanted cells, as evidenced by the absence of staining for Ki67, a marker of proliferation (Fig. 5). The implanted hESC-RPE expressed RPE65, an enzyme required for RPE to provide retinol to photoreceptors.[57] Most of the previous RPE transplantation procedures used cell suspension injections to deliver dissociated RPE cells into the SR area.[17,20,51] Injection of RPE cell suspensions may lead to the formation of isolated cell clumps that seldom develop into a polarized RPE monolayer structure.[40,41,43] Unattached cells may migrate to improper locations after injection, leading to serious complications, such as proliferative vitreal retinopathy.

The current study establishes that the implanted RPE performs photoreceptor outer segment phagocytosis for more than 5 months after implantation. This is demonstrated by the presence of host photoreceptor fragments inside the implanted RPE based on rhodopsin staining. Previous studies demonstrated phagocytosis of photoreceptor OS by implanted iris pigment epithelial cells[58] and human central nervous system stem cells in the RCS retina.[34] However, the investiga-

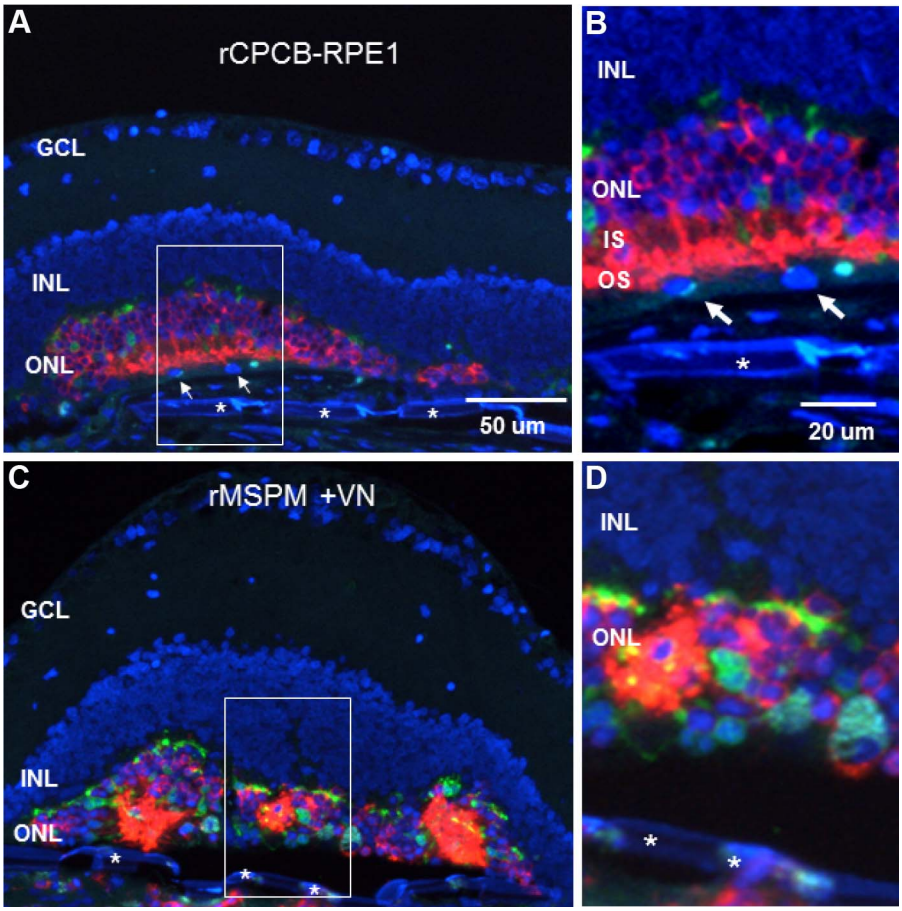

FIGURE 4. Photoreceptor rescue in RCS rats. Although rescue of rods and cones was found in both rCPCB-RPE1– and rMSPM+VN–implanted animals, there was better differentiation and alignment of photoreceptors and IS and OS, observed in the rCPCB-RPE1–implanted rats. (**A**) Retina implanted with rCPCB-RPE1 stained with antibodies to rhodopsin (rods) and cone arrestin (cones). (**B**) Higher magnification image of (**A**) (area indicated by a *rectangle*). (**C**) Representative image of rMSPM+VN stained with antibodies to rhodopsin and cone arrestin. (**D**) Higher magnification image of (**C**) (area indicated by a *rectangle*). *White arrows* pointing to hESC-RPE cells; parylene membrane is indicated by *white asterisks*. Rhodopsin: *red*; cone arrestin: *green*, DAPI: *blue*.

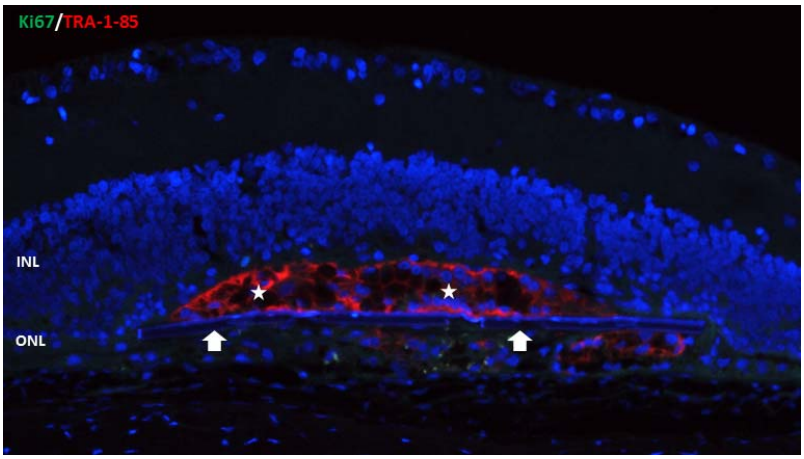

FIGURE 5. Absence of Ki67 staining in rCPCB-RPE1–implanted retina. Representative image of rCPCB-RPE1–implanted RCS rat eye tested for Ki67 staining at 21 weeks after implantation. No Ki67-positive cells (*green nuclei*) were found in the TRA-1-85 (human marker)–positive rCPCB-RPE1–implanted eyes. *Green*: Ki67 primary antibody and secondary antibody conjugated with FITC. *Red*: TRA-1-85 primary antibody and secondary antibody conjugated with rhodamine. *Blue*: DAPI nuclear stain. *White stars*: implanted hESC-RPE cells stained positively by TRA-1-85 (human cell marker). *White arrows*: membrane of rCPCB-RPE1 implant. Sections from mouse small intestine used as positive control showed numerous Ki67-positive cells (data not shown).

Investigative Ophthalmology & Visual Science

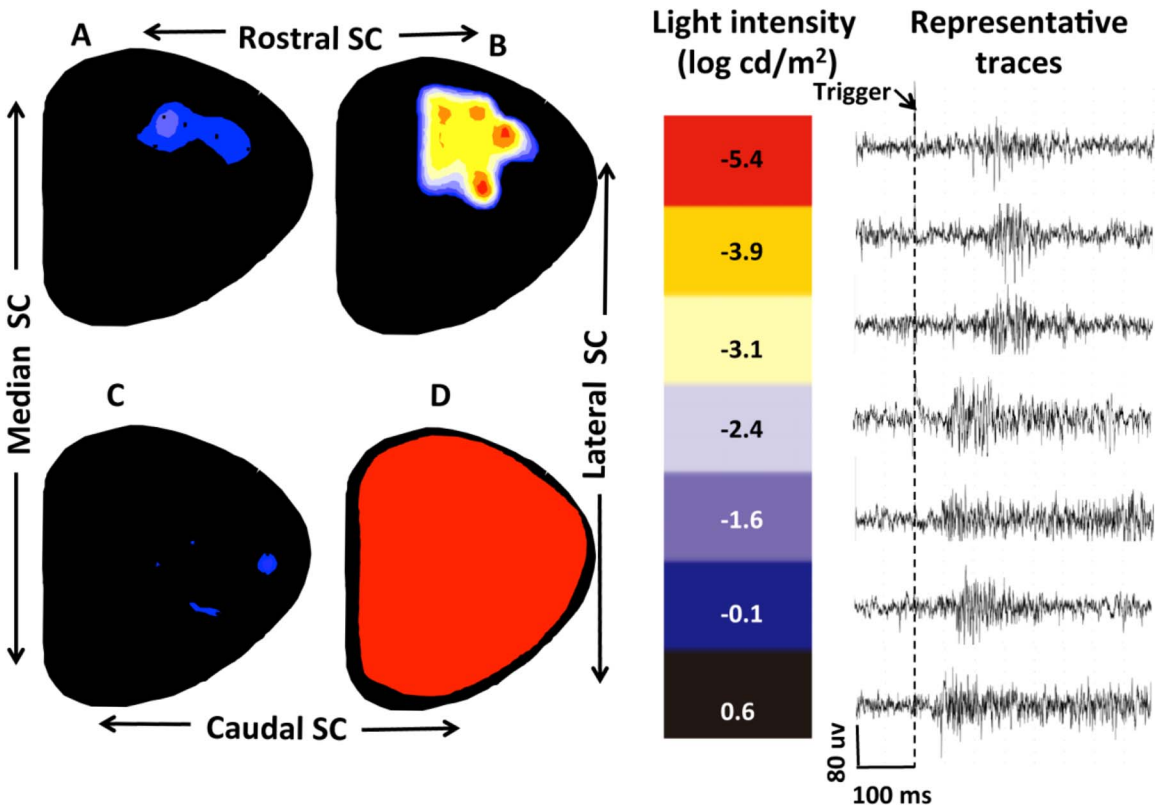

Figure 6. Diagram representing luminance threshold map of the SC of 6-month-old rats. The different colors represent the areas responding at different light intensity stimulus. The *black area* represents the area where no light response was observed even at the highest light level used (0.6 log cd/m^2). The low-light level responses were recorded from the SC of rCPCB-RPE1 animals (**B**) in an area that corresponded to the quadrant of the retina in which the implant was placed. During low-light level stimulation, no considerable visual activity was observed in the SC of rMSPM+VN–implanted rats (**A**) and nonimplanted RCS control animals (C). At the above light level, robust visual activities were recorded from all over the surface of the SC of normal control animals (**D**). Representative traces shown in the figure are samples taken from an rCPCB-RPE1–implanted animal at 6 months of age (~21 weeks postimplantation). Each trace includes the baseline activity 100 ms before light stimulation. The traces are arranged in correspondence with the light intensity level at which they were recorded.

tors used cell suspension injections in the above studies and hence normal RPE laminar structure was not achieved. Although Carr et al.[25] demonstrated phagocytic capability of the implanted RPE in RCS retina, they used induced pluripotent stem cell (IPS)-derived RPE that was delivered as cell suspension and the assays were conducted at a very early time point (approximately a week after implantation).

Detailed morphologic assessments demonstrated that the implanted rCPCB-RPE1 patch was capable of supporting and maintaining the functionality of the host photoreceptors. Quantitative estimation of the outer nuclear cell count from HE-stained retinal sections suggests a significant degree of photoreceptor preservation over the hESC-RPE implant. This can be considered a manifestation of the functionality of implanted hESC-RPE. However, it was not possible to achieve rescue of photoreceptors at the level observed in wild-type control rats; this can be explained in terms of surgical limitations and the progressive nature of photoreceptor degeneration in RCS rats. Due to surgical limitations, successful SR implantations are possible in RCS rats only after postnatal day 25. At this age, degeneration of the photoreceptors has already commenced.[59] According to LaVail,[59] degenerative activities in the RCS photoreceptors initiates in the second postnatal week. Assays of TUNEL staining indicate that photoreceptor cell death starts at postnatal (P)25. Hence, some limitations in the degree of ONL preservation can be expected even though the implanted hESC-RPE can survive and are functionally capable of maintaining normal retinal homeostasis.

Outer nuclear layer cell rescue was observed among both rCPCB-RPE1– and rMSPM+VN–implanted groups. A positive influence by the process of insertion of a parylene substrate in the photoreceptor preservation in RCS retina is not surprising, as previous studies have demonstrated sham surgery effects induced by any surgical intervention can lead to photoreceptor preservation and visual functional improvements.[60,61] This phenomenon can be explained in terms of a temporary rescue effect caused by the release of neurotrophic factors initiated by the surgical trauma.[60] Based on fetal retinal sheet transplantation studies, "sham surgery" effects are generally transient and their visual functional benefits are less robust when compared with the actual tissue implantation.[62] In most of the investigations that looked into the "sham surgery" effect, a temporary insult to the retina was induced by introducing a surgical tool or by creating an SR bleb. Contrary to this, in our experiments, the parylene substrate remains in the SR space in the entire period of study. This may lead to more sustained release of neurotrophic factors causing photoreceptor preservation and some visual functional benefits.

To obtain better insight into the mechanism of behavioral visual improvement observed in rCPCB-RPE1–implanted RCS rats, SC luminance threshold mapping was performed. Based on retinocollicular map properties,[54] it is possible to assess the functionality of photoreceptors that are preserved in a small area in the eye. The approach is suitable for assessing the

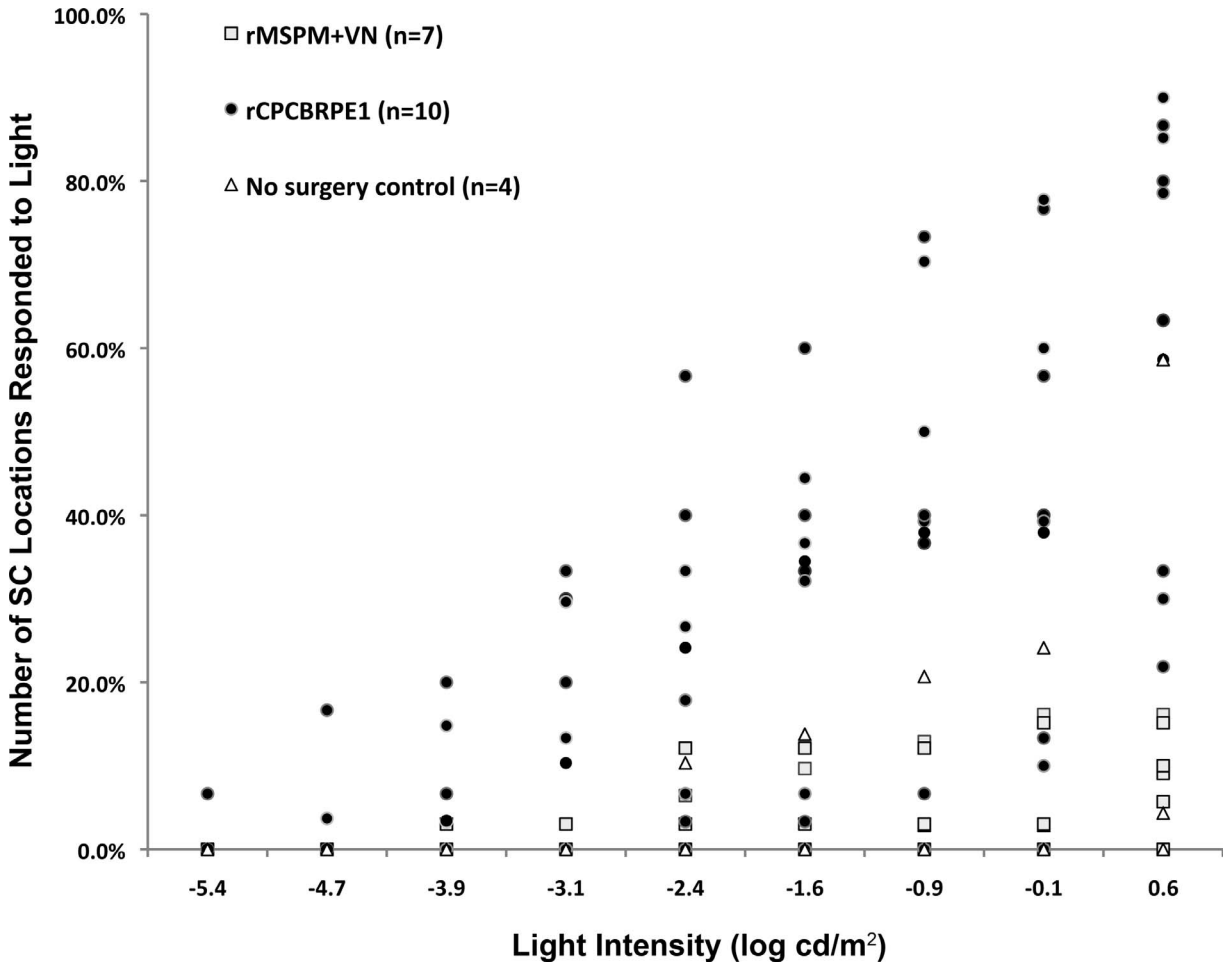

FIGURE 7. Superior colliculus luminance threshold mapping data from 6-month-old dystrophic RCS rats. Rats implanted with rCPCB-RPE1 had significantly higher number of SC locations that responded to light stimulation ($P < 0.05$, 1-way ANOVA followed by Bonferroni post hoc test, rMSPM+VN versus rCPCB-RPE1). These responses were recorded during low-light level stimulation (presumably rode-mediated responses), whereas, in the rMSPM+VN group and control (nonimplanted) RCS rats, responses were recorded from a fewer number of SC locations and only during higher light level stimulation (presumably cone responses). No statistical comparison was performed below −3.9 log cd/m² because SC responses at this light level could be recorded only from rCPCB-RPE1 animals.

functionality of the rescued photoreceptors (including rods and cones)[55] that are located in a small area overlying the implant. Our morphologic analysis demonstrated higher rod/cone ratio in rCPCB-RPE1–implanted rats (Table 2; Fig. 3). Some samples in rCPCB-RPE1 group showed more than three times more rods than cones, whereas no samples in the rMSPM+VN group showed rod/cone ratios at this level. To corroborate this, our SC mapping study showed robust visual preservation in rCPCB-RPE1–implanted animals during low-light level stimulation. The responses recorded during such low-light level stimulation can be considered rod-mediated based on our previous studies conducted in normal (nondegenerate) laboratory rats.[55] Interestingly, these responses were all recorded from an area of the SC that corresponded to the quadrant of the eye in which the rCPCB-RPE1 implant was placed (see Fig. 6B). In addition to the higher rod/cone ratio, the ONL layer overlying the rCPCB-RPE1 implant showed better differentiation and alignment of photoreceptors, which includes their IS (Figs. 4A, 4B). Based on the above observations, a direct contribution of the hESC-RPE in the preservation of visual function among rCPCB-RPE1–implanted animals can be inferred.

Despite the poorly laminated structure of the retina, most of the rMSPM+VN animals exhibited approximately equal numbers of rod and cone photoreceptors. However, SC visual activity in these animals (group 1) was not as robust as was observed in the rCPCB-RPE1–implanted animals (group 2). Responses in rMSPM+VN–implanted animals were recorded only during higher light level stimulation and hence presumed to be mediated by rescued cone photoreceptors.

In our current investigation, both implantation groups (rCPCB-RPE1 and rMSPM+VN) displayed some degree of cellular reaction surrounding the implant. Previous studies performed in rabbits suggested that episcleral fibroblast migration through an open scleral wound plays a role in the development of the intraocular fibrous proliferation.[63] The transscleral approach used for the implantation surgeries was ascribed a role for the cellular reactions observed in a similar study conducted by our group using athymic nude rats.[49] Because of the small size of the rat eye, a transscleral approach is required for rat implantation surgeries. This can provide the opportunity for infiltration of cells from outside the retina eventually leading to cellular reactions. However, because a different surgical approach will be used for the human eye, occurrence of the above phenomenon is not anticipated during clinical trials.

In conclusion, we have shown that a polarized hESC-RPE monolayer supported by a biocompatible substrate (rCPCB-

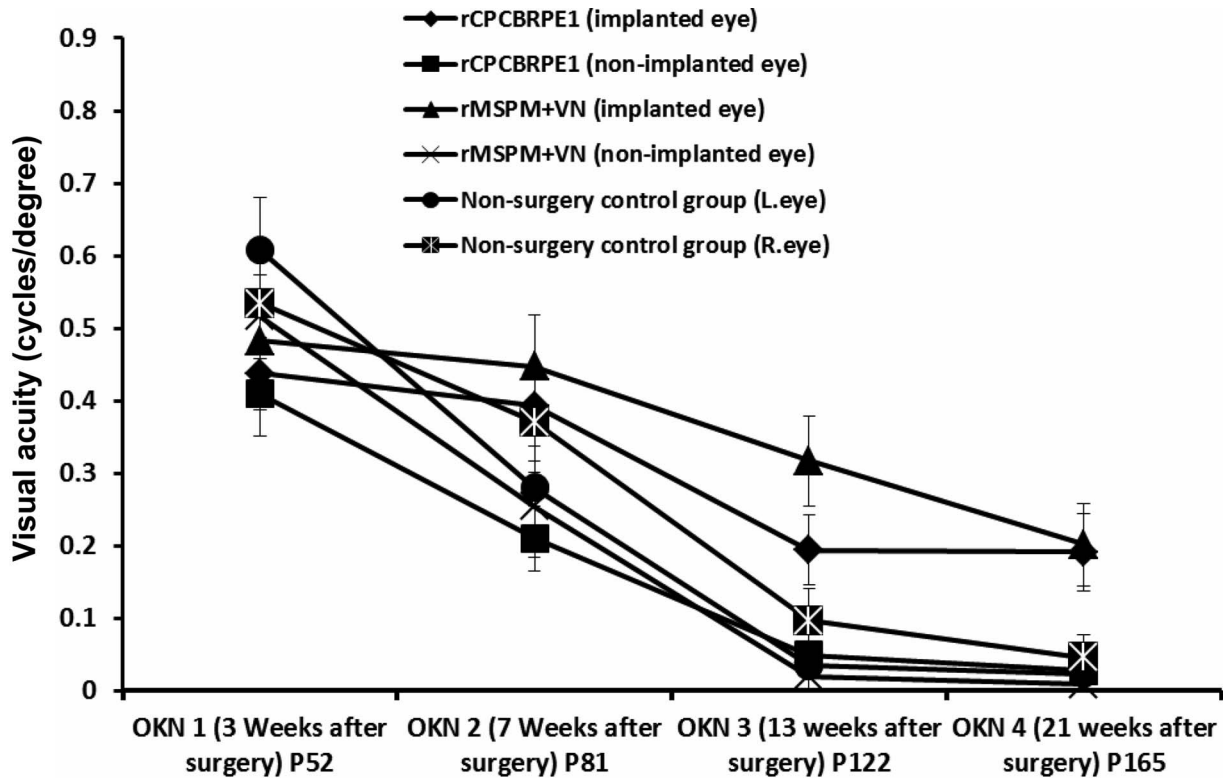

Figure 8. Optokinetic testing was performed in RCS rats at different time points after surgery. During the last two time points (13 weeks and 21 weeks postsurgery), eyes that received subretinal implantation of rMSPM+VN or rCPCB-RPE1 both showed better visual acuity compared with the nonimplanted eyes ($P < 0.05$, paired *t*-test). No considerable OKN activity was observed in the control animals (nonimplanted RCS rats) during the above time points. No significant differences between rMSPM+VN– and rCPCP-RPE1–implanted animals were observed in the degree of OKN improvement.

RPE1 implants) can survive and function to support the host photoreceptors after implantation in RCS rats. Our study suggests that rCPCB-RPE1 implants may be considered suitable for treatment strategy to slow the progression of dry-type AMD.

Acknowledgments

The authors thank colleagues Sherry Hikita and Linc Johnson for their valuable contributions in the manuscript and for the technical assistance from Zhenhai Chen, Anthony Rodriquez, Eric Barron, and Xiaopeng Wang.

Supported by Grant DR1-01444 from the California Institute for Regenerative Medicine and by the Institute for Collaborative Biotechnologies at the University of California Santa Barbara through Grant W911NF-09-0001 from the U.S. Army Research Office. Supported by an unrestricted departmental grant from Research to Prevent Blindness, New York, New York, United States.

Disclosure: **B.B. Thomas**, None; **D. Zhu**, None; **L. Zhang**, None; **P.B. Thomas**, None; **Y. Hu**, None; **H. Nazari**, None; **F. Stefanini**, None; **P. Falabella**, None; **D.O. Clegg**, Regenerative Patch Technologies, LLC. (I), P; **D.R. Hinton**, Regenerative Patch Technologies, LLC. (I), P; **M.S. Humayun**, Regenerative Patch Technologies, LLC. (I), P

References

1. Ambati J, Fowler BJ. Mechanisms of age-related macular degeneration. *Neuron*. 2012;75:26–39.
2. Fine SL, Berger JW, Maguire MG, Ho AC. Age-related macular degeneration. *N Engl J Med*. 2000;342:483–492.
3. Klein R, Peto T, Bird A, Vannewkirk MR. The epidemiology of age-related macular degeneration. *Am J Ophthalmol*. 2004; 137:486–495.
4. Ciulla TA, Rosenfeld PJ. Antivascular endothelial growth factor therapy for neovascular age-related macular degeneration. *Curr Opin Ophthalmol*. 2009;20:158–165.
5. Biarnes M, Mones J, Alonso J, Arias L. Update on geographic atrophy in age-related macular degeneration. *Optom Vis Sci*. 2011;88:881–889.
6. Nowak JZ. Age-related macular degeneration (AMD): pathogenesis and therapy. *Pharmacol Rep*. 2006;58:353–363.
7. da Cruz L, Chen FK, Ahmado A, Greenwood J, Coffey P. RPE transplantation and its role in retinal disease. *Prog Retin Eye Res*. 2007;26:598–635.
8. Jayakody SA, Gonzalez-Cordero A, Ali RR, Pearson RA. Cellular strategies for retinal repair by photoreceptor replacement. *Prog Retin Eye Res*. 2015;46:31–66.
9. Kamao H, Mandai M, Okamoto S, et al. Characterization of human induced pluripotent stem cell-derived retinal pigment epithelium cell sheets aiming for clinical application. *Stem Cell Reports*. 2014;2:205–218.
10. Mead B, Berry M, Logan A, Scott RA, Leadbeater W, Scheven BA. Stem cell treatment of degenerative eye disease. *Stem Cell Res*. 2015;14:243–257.
11. Nazari H, Zhang L, Zhu D, et al. Stem cell based therapies for age-related macular degeneration: the promises and the challenges. *Prog Retin Eye Res*. 2015;48:1–39.
12. Nguyen HV, Li Y, Tsang SH. Patient-specific iPSC-derived RPE for modeling of retinal diseases. *J Clin Med*. 2015;4:567–578.
13. Schwartz SD, Regillo CD, Lam BL, et al. Human embryonic stem cell-derived retinal pigment epithelium in patients with

age-related macular degeneration and Stargardt's macular dystrophy: follow-up of two open-label phase 1/2 studies. *Lancet*. 2015;385:509–516.

14. Sun J, Mandai M, Kamao H, et al. Protective effects of human iPS-derived retinal pigmented epithelial cells in comparison with human mesenchymal stromal cells and human neural stem cells on the degenerating retina in rd1 mice. *Stem Cells*. 2015;33:1543–1553.
15. Wright LS, Phillips MJ, Pinilla I, Hei D, Gamm DM. Induced pluripotent stem cells as custom therapeutics for retinal repair: progress and rationale. *Exp Eye Res*. 2014;123:161–172.
16. Zarbin M. Cell-based therapy for degenerative retinal disease. *Trends Mol Med*. 2016;22:115–134.
17. Coffey PJ, Girman S, Wang SM, et al. Long-term preservation of cortically dependent visual function in RCS rats by transplantation. *Nat Neurosci*. 2002;5:53–56.
18. Tezel TH, Del Priore LV, Berger AS, Kaplan HJ. Adult retinal pigment epithelial transplantation in exudative age-related macular degeneration. *Am J Ophthalmol*. 2007;143:584–595.
19. Gabrielian K, Oganesian A, Patel SC, Verp MS, Ernest JT. Cellular response in rabbit eyes after human fetal RPE cell transplantation. *Graefes Arch Clin Exp Ophthalmol*. 1999;237:326–335.
20. Carr AJ, Vugler A, Lawrence J, et al. Molecular characterization and functional analysis of phagocytosis by human embryonic stem cell-derived RPE cells using a novel human retinal assay. *Mol Vis*. 2009;15:283–295.
21. Idelson M, Alper R, Obolensky A, et al. Directed differentiation of human embryonic stem cells into functional retinal pigment epithelium cells. *Cell Stem Cell*. 2009;5:396–408.
22. Klimanskaya I, Hipp J, Rezai KA, West M, Atala A, Lanza R. Derivation and comparative assessment of retinal pigment epithelium from human embryonic stem cells using transcriptomics. *Cloning Stem Cells*. 2004;6:217–245.
23. Osakada F, Ikeda H, Mandai M, et al. Toward the generation of rod and cone photoreceptors from mouse, monkey and human embryonic stem cells. *Nat Biotechnol*. 2008;26:215–224.
24. Vugler A, Carr AJ, Lawrence J, et al. Elucidating the phenomenon of HESC-derived RPE: anatomy of cell genesis, expansion and retinal transplantation. *Exp Neurol*. 2008;214:347–361.
25. Carr AJ, Vugler AA, Hikita ST, et al. Protective effects of human iPS-derived retinal pigment epithelium cell transplantation in the retinal dystrophic rat. *PLoS One*. 2009;4:e8152.
26. Maeda T, Lee MJ, Palczewska G, et al. Retinal pigmented epithelial cells obtained from human induced pluripotent stem cells possess functional visual cycle enzymes in vitro and in vivo. *J Biol Chem*. 2013;288:34484–34493.
27. Assawachananont J, Mandai M, Okamoto S, et al. Transplantation of embryonic and induced pluripotent stem cell-derived 3D retinal sheets into retinal degenerative mice. *Stem Cell Reports*. 2014;2:662–674.
28. Baker PS, Brown GC. Stem-cell therapy in retinal disease. *Curr Opin Ophthalmol*. 2009;20:175–181.
29. Forest DL, Johnson LV, Clegg DO. Cellular models and therapies for age-related macular degeneration. *Dis Model Mech*. 2015;8:421–427.
30. Francis PJ, Wang S, Zhang Y, et al. Subretinal transplantation of forebrain progenitor cells in nonhuman primates: survival and intact retinal function. *Invest Ophthalmol Vis Sci*. 2009;50:3425–3431.
31. Inoue Y, Iriyama A, Ueno S, et al. Subretinal transplantation of bone marrow mesenchymal stem cells delays retinal degeneration in the RCS rat model of retinal degeneration. *Exp Eye Res*. 2007;85:234–241.
32. Lawrence JM, Sauve Y, Keegan DJ, et al. Schwann cell grafting into the retina of the dystrophic RCS rat limits functional deterioration. Royal College of Surgeons. *Invest Ophthalmol Vis Sci*. 2000;41:518–528.
33. Luo J, Baranov P, Patel S, et al. Human retinal progenitor cell transplantation preserves vision. *J Biol Chem*. 2014;289:6362–6371.
34. McGill TJ, Cottam B, Lu B, et al. Transplantation of human central nervous system stem cells - neuroprotection in retinal degeneration. *Eur J Neurosci*. 2012;35:468–477.
35. Pearson RA, Hippert C, Graca AB, Barber AC. Photoreceptor replacement therapy: challenges presented by the diseased recipient retinal environment. *Vis Neurosci*. 2014;31:333–344.
36. Thumann G, Salz AK, Walter P, Johnen S. Preservation of photoreceptors in dystrophic RCS rats following allo- and xenotransplantation of IPE cells. *Graefes Arch Clin Exp Ophthalmol*. 2009;247:363–369.
37. Wang S, Girman S, Lu B, et al. Long-term vision rescue by human neural progenitors in a rat model of photoreceptor degeneration. *Invest Ophthalmol Vis Sci*. 2008;49:3201–3206.
38. Lee E, Maclaren RE. Sources of retinal pigment epithelium (RPE) for replacement therapy. *Br J Ophthalmol*. 2010;95:445–449.
39. Schwartz SD, Hubschman JP, Heilwell G, et al. Embryonic stem cell trials for macular degeneration: a preliminary report. *Lancet*. 379:713–720.
40. Phillips SJ, Sadda SR, Tso MO, Humayan MS, de Juan E Jr, Binder S. Autologous transplantation of retinal pigment epithelium after mechanical debridement of Bruch's membrane. *Curr Eye Res*. 2003;26:81–88.
41. Shiragami C, Matsuo T, Shiraga F, Matsuo N. Transplanted and repopulated retinal pigment epithelial cells on damaged Bruch's membrane in rabbits. *Br J Ophthalmol*. 1998;82:1056–1062.
42. Gullapalli VK, Sugino IK, Van Patten Y, Shah S, Zarbin MA. Impaired RPE survival on aged submacular human Bruch's membrane. *Exp Eye Res*. 2005;80:235–248.
43. Hynes SR, Lavik EB. A tissue-engineered approach towards retinal repair: scaffolds for cell transplantation to the subretinal space. *Graefes Arch Clin Exp Ophthalmol*. 2010;248:763–778.
44. Krishna Y, Sheridan C, Kent D, Kearns V, Grierson I, Williams R. Expanded polytetrafluoroethylene as a substrate for retinal pigment epithelial cell growth and transplantation in age-related macular degeneration. *Br J Ophthalmol*. 2011;95:569–573.
45. Lu L, Yaszemski MJ, Mikos AG. Retinal pigment epithelium engineering using synthetic biodegradable polymers. *Biomaterials*. 2001;22:3345–3355.
46. Tao S, Young C, Redenti S, et al. Survival, migration and differentiation of retinal progenitor cells transplanted on micro-machined poly(methyl methacrylate) scaffolds to the subretinal space. *Lab Chip*. 2007;7:695–701.
47. Thomson HA, Treharne AJ, Walker P, Grossel MC, Lotery AJ. Optimisation of polymer scaffolds for retinal pigment epithelium (RPE) cell transplantation. *Br J Ophthalmol*. 2009;95:563–568.
48. Lu B, Zhu D, Hinton D, Humayun MS, Tai YC. Mesh-supported submicron parylene-C membranes for culturing retinal pigment epithelial cells. *Biomed Microdevices*. 2012;14:659–667.
49. Diniz B, Thomas P, Thomas B, et al. Subretinal implantation of retinal pigment epithelial cells derived from human embryonic stem cells: improved survival when implanted as a monolayer. *Invest Ophthalmol Vis Sci*. 2013;54:5087–5096.
50. Strauss O. The retinal pigment epithelium in visual function. *Physiol Rev*. 2005;85:845–881.

Investigative Ophthalmology & Visual Science

51. Lu B, Malcuit C, Wang S, et al. Long-term safety and function of RPE from human embryonic stem cells in preclinical models of macular degeneration. *Stem Cells*. 2009;27:2126–2135.
52. Klimanskaya I. Retinal pigment epithelium. *Methods Enzymol*. 2006;418:169–194.
53. Thomas BB, Shi D, Khine K, Kim LA, Sadda SR. Modulatory influence of stimulus parameters on optokinetic head-tracking response. *Neurosci Lett*. 2010;479:92–96.
54. Siminoff R, Schwassmann HO, Kruger L. An electrophysiological study of the visual projection to the superior colliculus of the rat. *J Comp Neurol*. 1966;127:435–444.
55. Thomas BB, Aramant RB, Sadda SR, Seiler MJ. Light response differences in the superior colliculus of albino and pigmented rats. *Neurosci Lett*. 2005;385:143–147.
56. Thomas BB, Seiler MJ, Sadda SR, Aramant RB. Superior colliculus responses to light—preserved by transplantation in a slow degeneration rat model. *Exp Eye Res*. 2004;79:29–39.
57. Cideciyan AV, Aleman TS, Boye SL, et al. Human gene therapy for RPE65 isomerase deficiency activates the retinoid cycle of vision but with slow rod kinetics. *Proc Natl Acad Sci U S A*. 2008;105:15112–15117.
58. Schraermeyer U, Kociok N, Heimann K. Rescue effects of IPE transplants in RCS rats: short-term results. *Invest Ophthalmol Vis Sci*. 1999;40:1545–1556.
59. LaVail MM. Analysis of neurological mutants with inherited retinal degeneration. Friedenwald lecture. *Invest Ophthalmol Vis Sci*. 1981;21:638–657.
60. Aramant RB, Seiler MJ. Progress in retinal sheet transplantation. *Prog Retin Eye Res*. 2004;23:475–494.
61. Silverman MS, Hughes SE. Photoreceptor rescue in the RCS rat without pigment epithelium transplantation. *Curr Eye Res*. 1990;9:183–191.
62. Thomas BB, Aramant RB, Sadda SR, Seiler MJ. Retinal transplantation. A treatment strategy for retinal degenerative diseases. *Adv Exp Med Biol*. 2006;572:367–376.
63. Lee SY, Ryan SJ. Pathophysiology of ocular trauma. In: Ryan SJ, Schachat AP, Wilinson CP, Hinton DR, Sadda SR, Wiedemann P, ed. *Retina.* 5th ed. London: W.B. Saunders; 2013:1647–1655.

Investigative Ophthalmology & Visual Science